Spectrochimica Acta Part B 120 (2016) 19–29

Contents lists available at ScienceDirect

Spectrochimica Acta Part B

journal homepage: www.elsevier.com/locate/sab

Application of distance correction to ChemCam laser-induced breakdown spectroscopy measurements

A. Mezzacappa [a], N. Melikechi [a,*], A. Cousin [b], R.C. Wiens [b], J. Lasue [c], S.M. Clegg [b], R. Tokar [d], S. Bender [d], N.L. Lanza [b], S. Maurice [c], G. Berger [c], O. Forni [c], O. Gasnault [c], M.D. Dyar [e], T. Boucher [e], E. Lewin [f], C. Fabre [g], the M.S.L. Science Team

[a] Optical Science Center for Applied Research, Delaware State University, Dover, DE 19901, USA
[b] Los Alamos National Laboratory, Los Alamos, NM, USA
[c] Institut de Recherche en Astophysique et Planetologie (IRAP), Universite Paul Sabatier, Toulouse, France
[d] Planetary Science Institute, Flagstaff, AZ, USA
[e] Dept. of Astronomy, Mount Holyoke College, South Hadley, MA, USA
[f] Institut des Sciences de la Terre, Universite' Grenoble I-CNRS, Grenoble, France
[g] CNRS, Georessources, Vandoeuvre les Nancy, France

ARTICLE INFO

Article history:
Received 12 August 2015
Received in revised form 16 March 2016
Accepted 16 March 2016
Available online 4 April 2016

Keywords:
Stand-off laser-induced breakdown spectroscopy (ST-LIBS)
Mars
Dust
Calibration
Geological analysis

ABSTRACT

Laser-induced breakdown spectroscopy (LIBS) provides chemical information from atomic, ionic, and molecular emissions from which geochemical composition can be deciphered. Analysis of LIBS spectra in cases where targets are observed at different distances, as is the case for the ChemCam instrument on the Mars rover Curiosity, which performs analyses at distances between 2 and 7.4 m is not a simple task. In our previous work we showed that spectral distance correction based on a proxy spectroscopic standard created from first-shot dust observations on Mars targets ameliorates the distance bias in multivariate-based elemental-composition predictions of laboratory data. In this work, we correct an expanded set of neutral and ionic spectral emissions for distance bias in the ChemCam data set. By using and testing different selection criteria to generate multiple proxy standards, we find a correction that minimizes the difference in spectral intensity measured at two different distances and increases spectral reproducibility. When the quantitative performance of distance correction is assessed, there is improvement for SiO_2, Al_2O_3, CaO, FeOT, Na_2O, K_2O, that is, for most of the major rock forming elements, and for the total major-element weight percent predicted. However, for MgO the method does not provide improvements while for TiO_2, it yields inconsistent results. In addition, we have observed that many emission lines do not behave consistently with distance, evidenced from laboratory analogue measurements and ChemCam data. This limits the effectiveness of the method.

1. Introduction

Laser-induced breakdown spectroscopy (LIBS) has utility as a stand-off elemental composition technique, and has been demonstrated to be effective for a variety of applications. LIBS uses an intense laser [1] to irradiate, ablate, and break down chemical bonds in a sample, creating a weakly ionized and short lived plasma. Light emitted by this plasma is collected and transmitted to a spectrometer. Spectral lines indicate chemical composition and abundance of elements [2–5]. In a laboratory setting, it has been shown that stand-off LIBS (ST-LIBS) can identify metals, [6] energetic materials [7], nuclear fuel bi-products [8], biological materials [9] elemental compositions of archeological artifacts [10], subtle compositions of rock type under terrestrial [11] and lunar conditions [12]. In the field, LIBS has been used to monitor the effluent of a coal gasification plant [3]. A telescopic ST-LIBS system was employed at the THORP nuclear reprocessing plant to identify an unknown solid build up as zirconium molybdate [13]. Currently, ST-LIBS is being utilized for Mars exploration. The Curiosity rover that landed on Mars in 2012 is using ST-LIBS as part of the ChemCam instrument, which has provided a means to analyze several thousand locations on rocks and soils. ChemCam has analyzed rock outcrop compositional diversity [14–16] and soil diversity and hydration [17,18] from Curiosity's exploration of Gale crater. As fielded application of ST-LIBS grows, so too does the modality of application.

ST-LIBS often requires variation in measurement distance between the laser and its targets from one measurement to the next measurement, which presents an analytical challenge when comparing spectral results gleaned from these slightly different experimental configurations. Changes in distance are accompanied by other variable experimental parameters due to soil and rock diversity such as

* Corresponding author at: Delaware State University, 1200 N DuPont Hwy, Dover, DE 19901, USA.
E-mail address: nmelikechi@desu.edu (N. Melikechi).

http://dx.doi.org/10.1016/j.sab.2016.03.009
0584-8547/

surface texture and grain size along with consistency of focal position with respect to the sample surface. Salle et al. 2007 [19] conclude their review of ST-LIBS by citing the problem of variable distance as a future hurdle for the technique. Indeed, several authors have investigated the complexity of using an ST-LIBS instrument to take measurements at different distances [20–22]. In these studies the behavior of ST-LIBS signals from metal samples at different distance was investigated, and even though the same aluminum lines were investigated, Gaona et al. [20] and Palanco et al. [22] found differences in behavior attributable to different rates of sample ablation even with constant irradiance. Aguilera et al., 2008 (part 2) [23] uses the Curve of Growth method to predict with reasonable accuracy the emission intensities at different focusing distances for gated LIBS plasmas in simple samples, the spectra of which were free of matrix effects. While this technique is effective, due to the need for time-gated plasma detection and a priori knowledge of the concentration it is not applicable to ChemCam. The related problem of defocusing has also been investigated [6,24–26]. An expanded description of distance behaviors with distance, given by Melikechi et al., 2014 [27], evidences a variety of line behaviors.

In our previous work [27] using the ChemCam instrument we gave a proof of concept for distance correction with a proxy spectroscopic standard based on martian dust. The distance correction model relies on the fact that fine dust, presumed to be of globally uniform composition [28,29], coats all materials on Mars—rocks as well as soils. The single-shot spectral measurement capability of this instrument has provided the elemental composition of this dust, observed with the first several laser pulses of a laser burst that normally consists of 30 shots; often up to the first 5 spectra are similar to that of the global martian fine dust. The first laser shot on each location thus tends to reflect a re-occurring composition. Melikechi et al. 2014 [27] used distance-insensitive ratios of emission lines to identify pure Martian dust spectra and reject first-shot spectra with features representing contributions from underlying rocks and soils. After discrimination the dust forms an ersatz standard which is used to provide a distance correction. Distance calibrations are found for individual emission lines. When this line-specific distance calibration is applied to laboratory data, the correction improves the reproducibility of spectra observed at different distances. Partial Least Squares multivariate regression (PLS) is used to predict major-element abundances from spectra based on a model built on a training set of spectra from standards of known compositions. The model correlates pixel intensity and elemental abundance by creating a coefficient for every pixel/spectral channel, referred to as loadings [37]. The quantitative results from PLS converge toward the true compositions after distance correction with this method. These results illustrate the utility of the method for ChemCam data and other applications, including terrestrial ST-LIBS.

In this paper, we apply the discrimination method from [27] to ChemCam first shot spectra from the first 360 sols (solar days on Mars) and laboratory analogue measurements to test the model of distance correction. With the data available from Mars, we then assess distance correction using ChemCam spectra from the first 585 sols of the mission. Only first shot spectra that satisfy the set of criteria defined in Section 2 are used to generate distance calibration curves specific for each emission line. All elements with a non-trivial and reproducible distance bias are corrected. The method is partially

Table 1
Lists all element emission lines under consideration.

Consistently behaved emissions

Emission line & wavelength (nm)		Percent error	Emission line & wavelength (nm)		Percent error	Emission line & wavelength (nm)		Percent error
Fe I	404.7	5.03	Ti II	307.95	34.78	Al I	394.56	32.69
Fe I	406.23	7.24	Ti II	325.3	23.10	Al I	396.21	17.93
Fe I	425.2	29.13	Ti II	335.04	17.91	Al II	705.85	22.86
Fe I	427.3	18.23						
Fe I	432.7	6.47	Ca I	422.79	7.31	Mg II	448.2	2.38
Fe I	438.48	6.51	Ca I	443.6	8.62	Mg I	517.4	13.48
Fe I	440.6	7.91	Ca I	445.6	9.32	Mg I	518.5	16.42
			Ca I	616.3	8.52			
Na I	589	12.35	Ca I	649.5	26.78	Si I	288.2	12.19
Na I	589.6	36.41				Si II	412.92	11.46
Na I	818.55	14.82	K I	766.7	15.13	Si II	413.42	8.55
Na I	819.71	6.08	K I	770.11	15.79			

Inconsistently behaved emissions

Emission line & wavelength (nm)		Percent Error	Emission line & wavelength (nm)		Percent Error	Emission line & wavelength (nm)		Percent Error
Fe I	426.2	13.92	Ti II	306.7	39.24	Si I	250.69	15.83
Fe I	302.2	18.74	Ti II	307.3	58.58	Si I	251.6	10.10
Fe II	275.01	11.10	Ti II	307.6	43.81	Si I	252.37	7.95
Fe II	263.2	7.02	Ti II	308.89	23.10	Si I	252.9	10.66
Fe I	260	14.11	Ti II	323	58.58	Si I	390.66	21.12
Fe II	256.3	17.67	Ti II	324	43.81	Si II	634.88	7.62
Fe II	274	9.36	Ti II	324.2	34.78	Si II	637.2	17.03
Fe II	274.8	11.74	Ti II	324.9	13.71			
Fe II	275.65	9.88	Ti II	334.2	34.95	Ca II	315.98	10.95
Fe I	407.3	8.50	Ti II	336.2	15.89	Ca II	318.02	10.33
Fe I	441.6	12.78	Ti II	337.4	11.12	Ca II	396.96	4.45
						Ca II	393.48	3.67
Al I	308.31	25.90	Mg II	280.3	3.83	Ca I	526.6	8.29
Al I	309.21	13.77	Mg I	285.3	11.23	Ca I	612.3	14.20
Al II	704.4	17.85	Mg II	279.1	28.62	Ca I	646.3	17.56
			Mg II	279.6	3.95	Ca I	644.2	12.81
			Mg II	279.8	13.82			

These lines are selected as the primary drivers in quantitative analysis using PLS. Table (a) gives lines which are reproducible with distance. (b) Gives lines which are not reproducible with distance. To characterize these lines they are fit with a Lorentz function. The error for fits of both groups of lines given is computed from the error with respect to the full width at half maximum of the emission line and the error with respect to the intensity of the line.

Table 2
Ratios with high signal to noise and no saturation comprising the selection parameters of the proxy standard which is found as optimal. The selection values and the standard deviation among the ratios of all first shot measurements are given. The upper-state transition-energy difference is given as well. The stability of an electronic transition correlates negatively with the upper state transition energy. Under local thermal equilibrium the intensity ratio is expected to be less sensitive to fluctuations in plasma temperature for emission lines with a small difference in upper transition energy. [34].

Ratio set 4	Selection values		One standard deviation	Delta E (eV)
	Low	High		
Mg_{448}/Si_{288}	0.748	1.246	0.291	6.55
Fe_{260}/Si_{288}	1.527	2.546	1.165	0.60
Na_{589}/Ca_{397}	2.328	3.881	0.499	2.91
Al_{396}/Si_{288}	1.620	2.700	0.355	1.94
Mg_{448}/Fe_{260}	1.373	2.288	0.427	6.86
Ca_{397}/Al_{396}	3.010	5.016	0.716	1.88
Ca_{397}/K_{766}	1.100	1.833	0.281	3.40
Na_{589}/K_{766}	3.382	5.637	0.481	0.49
Ca_{397}/Si_{288}	0.015	0.025	0.010	0.06
K_{766}/Si_{288}	3.621	6.035	1.378	3.47
$(Fe_{260} + Mg_{448})/Si_{288}$	2.265	3.775	1.246	0.31 & 6.55
Ti_{335}/Si_{288}	0.428	0.714	0.234	1.33

successful in providing an appropriate distance correction for ChemCam data. With the help of laboratory analogue measurements in addition to ChemCam data we note that many lines do not display universal trends with distance, which limits the utility, but provides further information on the subject of distance effects.

2. Proxy standard generation

ChemCam consists of a LIBS and a Remote Micro-Imager (RMI) instruments. The ChemCam LIBS instrument emits 1067 nm laser pulses with an energy ranging from 6.5 mJ to 14 mJ, with a pulse duration of 4.5 ns and a repetition rate of 3 Hz. It can fire 30–150 laser pulses at each interrogation point on targets located between 1.6 m and 7.4 m from it. The excitation laser and plasma light are respectively delivered and collected by a 110 mm diameter telescope. The focal position of the secondary mirror of the Schmidt–Cassegrain telescope is determined from the target distance as calculated from the parallax of the Navcam imagers with an error of +/− 5%, followed (for data through sol 801) by a fine focus obtained by utilizing a maximized return signal of a CW laser through the ChemCam telescope [30,31]. The spectrometers cover the ultraviolet (UV), violet-blue (VIO), and the remaining visible and near infrared (VNIR) spectral ranges, collectively from 240 to 905 nm [31]. The RMI instrument provides sub-millimeter resolution context images.

To begin, a subset of LIBS emission lines are selected from the first-shot observations, looking for the highest signal-to-noise levels, lowest errors of fitted emission lines and the strongest PLS loadings, as will be described below. Because loadings of the PLS algorithm are used to determine elemental abundances, correcting the lines representing the strongest loadings should ameliorate distance-based biases in the predictions of composition. The 75 lines considered and listed in Table 1 are emissions of the major-element cations (e.g., Si, Al, Fe, Mg, Ca, Na, K, Ti). Along with oxygen anions, these

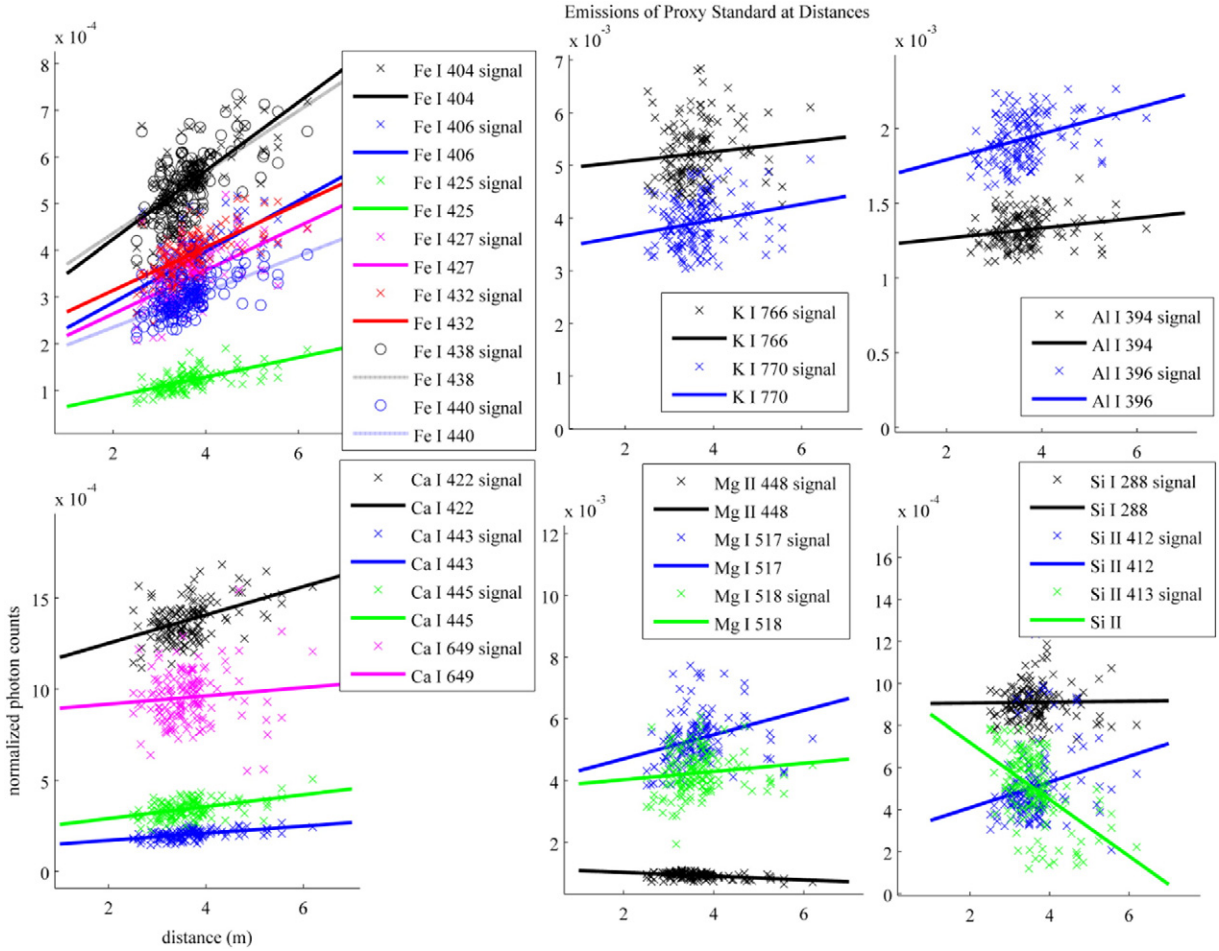

Fig. 1. Selected emission trends for optimized proxy standard. The y-axes are the photons per channel normalized to *norm3*.

Table 3
Emission lines, slopes and intercepts of linear calibration curves comprising the distance correction, and r-squared values of fits.

Proxy standard				
Signal		Slope(m^{-1})	Intercept	R^2
Fe I	404.7	7.33E−05	2.77E−04	0.4553
Fe I	406.2	5.44E−05	1.80E−04	0.4022
Fe I	425.2	2.10E−05	4.46E−05	0.3987
Fe I	427.3	4.66E−05	1.71E−04	0.2995
Fe I	432.7	4.60E−05	2.22E−04	0.4011
Fe I	438.5	6.56E−05	3.05E−04	0.3950
Fe I	440.6	3.81E−05	1.59E−04	0.4139
Si I	288.2	2.05E−06	9.02E−04	0.0002
Si II	412.9	6.10E−05	2.87E−04	0.0507
Si II	413.4	−1.35E−04	9.88E−04	0.2675
Al I	394.6	3.38E−05	1.20E−03	0.0408
Al I	396.2	8.66E−05	1.62E−03	0.1246
Ca I	422.8	7.77E−05	1.10E−03	0.2084
Ca I	443.6	1.96E−05	1.31E−04	0.2372
Ca I	445.6	3.26E−05	2.25E−04	0.1861
Ca I	649.5	2.26E−05	8.72E−04	0.0095
Mg II	448.2	−6.08E−05	1.14E−03	0.1577
Mg I	517.4	3.89E−04	3.93E−03	0.0698
Mg I	518.5	1.33E−04	3.76E−03	0.0149
K I	766.7	9.31E−05	4.88E−03	0.0106
K I	770.1	1.50E−04	3.36E−03	0.0434
Calibration data				
Signal		Slope(m^{-1})	Intercept	Average R^2
Al II	705.9	−4.29E−05	9.42E−04	0.4595
Ca I	616.3	6.15E−04	1.97E−03	0.6758
Na I	589	6.23E−04	1.05E−02	0.3888
Na I	589.6	3.93E−04	7.17E−03	0.3399
Na I	818.6	3.44E−04	2.07E−03	0.6719
Na I	819.7	8.34E−04	4.43E−03	0.6815

Calibrations divided within the table by the method of generation: from the Proxy Standard or the LANL calibration data.

major-element cations account for the majority of the mass fraction (generally >90%) of analyzed targets. These emission lines are representative of the entire frequency range:

(i) We consider only those emission lines with a signal-to-noise ratio greater than five where the signal is defined as the total intensity of the line minus the background, and noise as the fluctuation of the background around the emission line.
(ii) Fit error is carefully evaluated: Lines are fitted by a series of Lorentzian functions. The method used is that of the earlier work [27]. The Levenberg–Marquardt technique [36] is used to solve the least-squares problem, which optimizes the adjustment of Lorentz parameters to the data points. We chose to remove from consideration all lines with a fit error greater than 50%.
(iii) The lines considered are the prominent lines in the loadings of PLS predictions. They represent the driving components of where the spectra lie in feature space.

A subset of all first-shot LIBS spectra is selected to be used as a proxy standard, with the selections based on the best total signal, standard laser amplifier current, and yielding a composition within a narrow range around the expected composition, as described below. This selected subset of spectra is intended to serve as a standard composition at all distances. The selection process is as follows:

(i) The total photon count is the source radiance multiplied by the source area imaged, the solid viewing angle, the detector wavelength bin width, the integration time, and the system response [31,35]. We select spectra with total photon count higher than 2e + 13, typically representing a signal to noise greater than 5.
(ii) We select spectra which have been created with the laser operating at 95 amps of amplifier current; the resulting laser energy per pulse is ~14 mJ.1062 out of 2088 first-shot spectra satisfy this and the above conditions.
(iii) To generate a proxy standard with representative composition and mineralogy we use the discrimination method [27], first-shot spectra from sols 13–360 is normalized to the sum of photon intensities in all 2048 channels in each of the three spectrometers, referred to as norm3. (Norm3 normalization is utilized for all data unless otherwise statEd.) Proxy standards are a set of spectra within the first-shot dust measurements satisfying (i), (ii) and the selection parameters in Table 2, within +/−25% of the median value. Ratios in Table 2 utilize emission lines with high signal to noise without

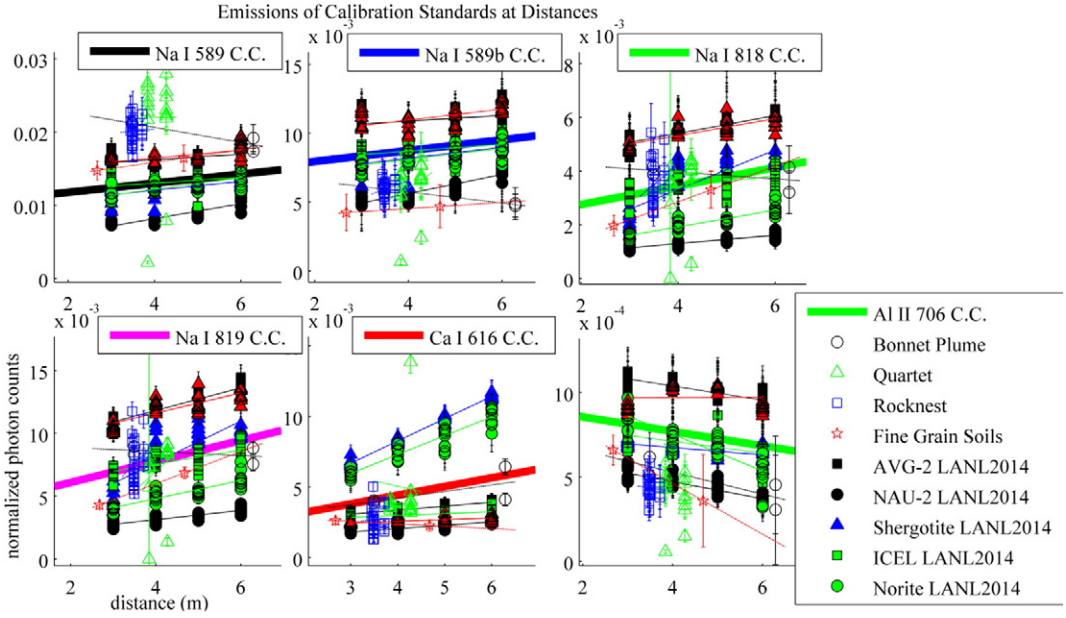

Fig. 2. Emission trends for LANL calibration data for selected lines. The y-axes are the photons per channel normalized to *norm3*.

Table 4
Mean composition of 1st shot dust measurements, from proxy standard generated using values in Table 1 generated with PLS1 multivariate regression, with the root mean square error product (RMSEP) of the model shown in the bottom row. Dust composition values are in weight percent; one standard deviation among the set is also shown.

Mean of PLS1 predictions for dust proxy standard composition distances									
Oxide predicted	SiO_2	TiO_2	$A1_2O_3$	FeOT	MgO	CaO	Na_2O	K_2O	Total
Dust proxy mean value	37.10	1.27	9.03	14.14	5.54	5.52	1.73	0.32	74.65
Dust proxy standard deviation	2.02	0.17	0.48	1.06	0.76	0.69	0.27	0.24	3.84
RMSEP	7.10	0.55	3.70	4.00	3.00	3.30	0.70	0.90	10.10

saturated lines.[1] Table 2 gives the discrimination selection values and set information. Of the 2088 initial spectra, 92 first shot spectra are retained. Fig. 1 shows distance calibration curves. Emission intensities of all spectra within the proxy standard are plotted with the distance of observation. A linear best fit is applied to generate calibration curves. Quadratic, cubic and exponential functions were also tested but none produced better fits than the linear one.

3. Selecting and implementing a proxy standard with ChemCam and laboratory data

We test provisional proxy standards, created by modifying ratios chosen for discrimination, on Mars data which has been directly observed with ChemCam on the surface of Mars. To select distance calibration targets from the ChemCam data set, targets must be observed over at least two distances and spectra taken at different raster points must be homogeneous. These include fine-grained soils which are observed in a blind targeting regime and other measurements during the rover's traverse from Yellow Knife bay toward Mount Sharp. These soils are identified via RMI and are distinguished from underlying coarse grains by hydrogen content and comparison of shot-to-shot elemental compositional variation. Fine-grained soils show homogeneous composition all along the traverse [18]. These fine-grained soils were targeted at many distances from 2.66 m to 5.28 m. Besides the soils, two additional targets that are used to test the distance correction are the rock targets Bonnet Plume and Square Top which were observed with LIBS at multiple distances. We also use laboratory data of geological standards taken at Los Alamos National Laboratory at different distances using an engineering model of ChemCam. The distance calibration suite is taken with 95 Amp. of laser amplifier current corresponding to ~14 mJ of laser energy. Five targets interrogated in the lab are AVG-2, NAU-2, Shergotite, ICEL, and Norite [35,37].

Calibration curves generated from proxy standard created with selection parameters in Table 2 best represent the distance effect seen in ChemCam targets on Mars as seen in linear best fits to emission intensities with distance of fine-grained soils. The fine-grained soils represent measurement of one sample at many distances, best representing the distance effects. Slopes of calibration curves of provisional proxy standards were compared with slopes of fits of emission lines in Table 1 of the fine-grained soils. Provisional proxy standard generated with low signal to noise lines only correct 11 lines for the fine-grained soils, while that generated with Table 2 corrects 23 lines. Because Table 2 ratios create the most accurate correction compared to other sets, we choose this set of spectra to be the proxy standard. We consider the difference in line intensity due to difference of measurement distance for each line measured on the same material. If applying the correction to the line increases this difference in either Bonnet Plume or the fine-grained soils, the line is eliminated from the correction. We keep only the calibrations which improve spectral reproducibility. Table 3 presents calibration curves and R squared values from the Ratio Set 4 proxy standard.

The laboratory calibration data is used as an additional check on the behavior of emission lines. If the behavior with distance of an emission line in Table 1 is consistent across the laboratory calibration targets, the fine-grained soils, and the Proxy Standard, it is listed in Table 1 as consistently behaved. If it is inconsistent across these it is listed in Table 1 as inconsistently behaved. There are exceptions for emission lines that are consistent with the behavior of lines from the fine-grained soils, the laboratory calibration data, and additionally Bonnet Plume, but disagree with only the calibration curve given by the proxy standard. In this case we use a calibration curve built from the average behavior with distance of the laboratory calibration targets, shown in Fig. 2. That is, the best linear fit of an emission line at observation distances of 3 m, 4 m, 5 m, and 6 m from each of the laboratory calibration targets is averaged to generate an average calibration curve. Table 3 provides distance calibration curves from the dust proxy standard and also calibration curves for Ca, Al and Na from the laboratory data. R squared values of best fits are given for proxy standard calibration curves. Average R squared values of the five best fits of the lab data are given. Ti lines are not added because the Ti lines in Table 1a have effectively no change with distance within the scatter of the data. Because all other lines considered are not consistent with distance, the 27 lines presented in Table 3 represent all lines that can be corrected within the original set.

In the first 360 sols we observed a consistent dust signal in the spectra from the first laser shot at each location, and this material is likely to be present everywhere on the surface of the planet, constituting an internal spectroscopic standard for ChemCam. The dust spectral signature used above has a composition determined by the partial least squares (PLS1) regression [35] used by the team between sols 385 and 1020, and is given in Table 4. The root mean square error product (RMSEP) of this calibration model is also given there. The compositional value for these oxides in the dust fluctuates less than 15% around a mean value. This composition has been studied extensively [32,33], and is found to be generally uniform at all Mars landing sites to date. Furthermore, by using a standard that is internal to the ChemCam data set, instrument collection geometry, instrument response, and laser characteristics remain constant, though the method does not rely on this.

4. Applying distance calibration curves to ChemCam LIBS data

The combined set of calibration curves in Table 3 is applied to the ChemCam targets as a distance correction. The spectra are considered at two distances and the observation made at the larger measurement distance is corrected to the distance of the shorter measurement distance. To demonstrate the correction, we use observations with a large enough difference in distance, greater than 2 m, to avoid results being obscured by variability in the spectral emissions. Square Top was observed at 2.43 m and 4.47 m and Bonnet Plume at 3.5 m and at 6.2 m. The fine-grained soils are observed at many distances, but here we use average spectra from 4.8 m and at 2.7 m. Distance correction is applied to these ChemCam targets by using the calibration curve of an emission line, generated by a linear best fit of emissions from proxy standard spectra at many distances. Each pixel that contributes to that individual emission line is scaled with this calibration curve. When

[1] Ratios comprised of different lines were tested for correction of fine-grained soils, the ratios in Table 2 represent the proxy standard which corrected the greatest number of lines.

these linear calibration curves are applied to homogeneous targets observed at multiple distances, spectral reproducibility, the equality of emission lines under different observation distances, is improved for all corrected lines. Fig. 3 shows spectral correction for the fine-grained soils, Bonnet Plume, and Square Top. The difference between the integrals of each emission line in the targets at near and far distances before

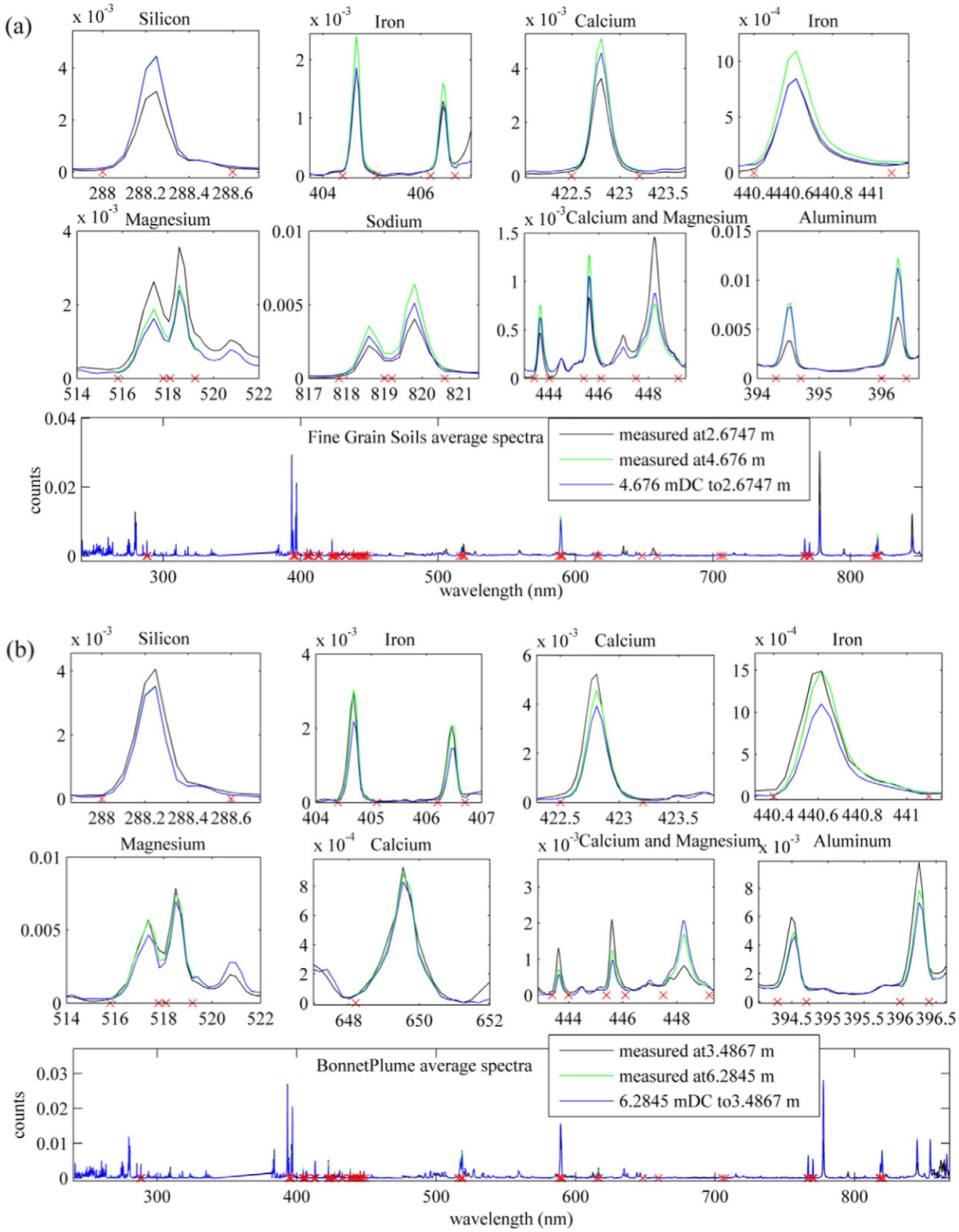

Fig. 3. ChemCam spectra with *norm3* normalization (a) Fines Corrected and Uncorrected, full spectra and vignettes (b) Bonnet 1 (ccam02171 #7 to ccam01149 #7) Corrected and Uncorrected, full spectra and vignettes (c) Square Top Corrected and Uncorrected, full spectra and vignettes. The grey line is the LIBS spectra measured at a distance of 2.67 m. The green one is the LIBS spectra of the same target measured at a distance of 4.67 m. The blue spectrum is the one calculated by correcting the spectrum measured at 4.67 m to 2.67 m. Following distance correction, the blue spectrum should translate closer to the grey one. If the correction was perfect, blue and grey spectra should be undistinguishable (as is almost the case for Si and to some extent Fe). For Mg, the blue spectrum is further away from the grey one than the green one, which shows that the method does not work for Mg.

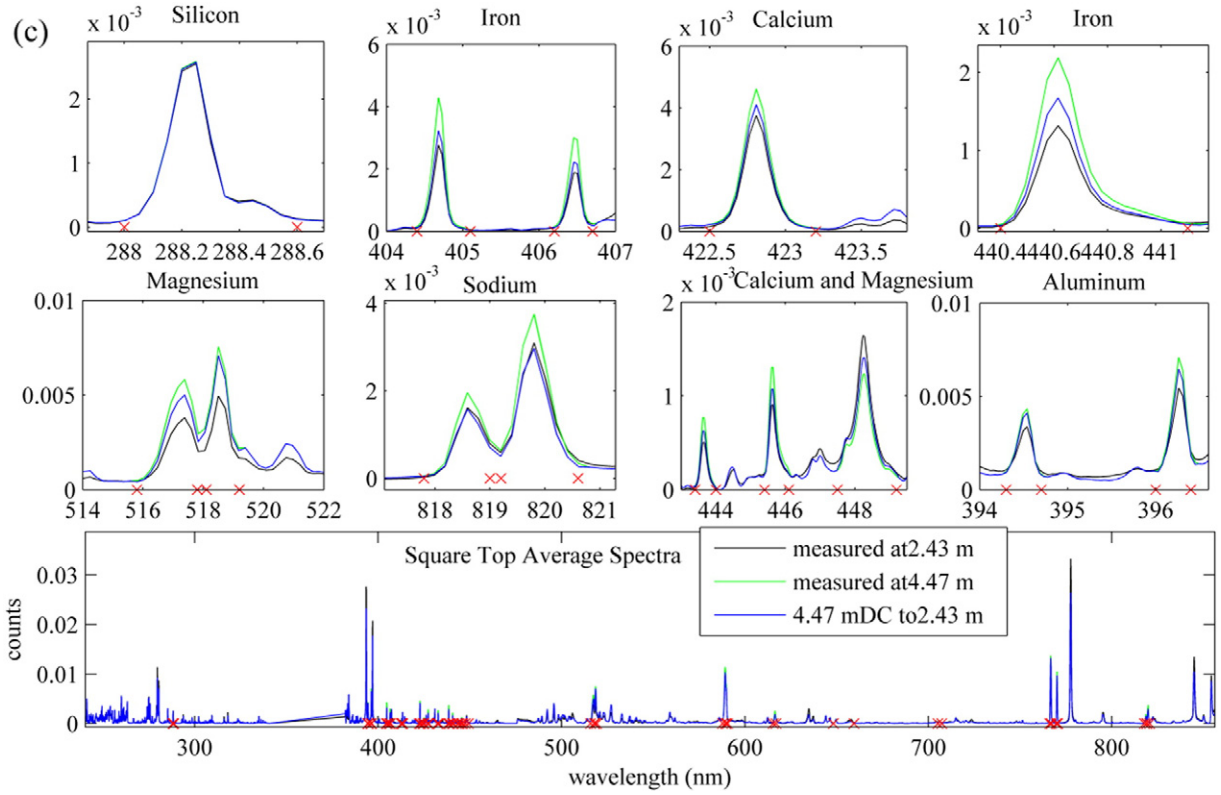

Fig. 3 (*continued*).

and after correction is presented in Fig. 4. As evidenced by Figs. 3 and 4 the correction reduces the difference due to distance for all the lines it is applied to. Perfect correction is impaired by other experimental parameters mentioned above.

The degree to which the spectral difference due to distance is removed varies for each target studied. Though all three targets represent similar distance ranges, the difference due to distance is variable; for example the iron signals in Square Top have a larger bias than those of the fine-grained soils or Bonnet Plume. In this case the fine-grained soils observe the most effective correction for iron signals because they have the most similar behavior to the proxy standard. Distance correction to silicon signals and aluminum signals provide partial correction for the total bias across all samples. The distance bias on calcium signals remains consistent across the three targets as does the effectiveness of the correction. Magnesium also has a distance bias which appears inconsistent across the targets, with the fine-grained soils having the greatest bias; for these lines the correction is most effective for Bonnet Plume. Sodium and potassium are addressed in the fine-grained soils and Square Top where they provide a partial correction for the total distance bias. This variety of behaviors among general trends with distance is not addressed here.

5. Results of distance correction on PLS predictions

ChemCam provides chemistry information about rock, soil, and dust targets in Gale Crater on Mars. The information gleaned from the spectrochemistry is then interpreted to determine the geological history of the area by inferring the mineralogy and mineral assemblages in the target. Rock types can be predicted using multivariate analysis techniques. PLS predicts major element abundances from spectra based on a multivariate linear regression model built on a training set [38]. Here we present the impact of measurement distance on PLS predictions of ChemCam targets from a model built with standards at one distance–3 m–and improvements to PLS by applying distance correction.

The PLS model used for prediction here was created from a database of 69 standards observed at a 3 m distance with an engineering model of ChemCam. This model is used to predict targets observed by the ChemCam instrument on Mars: the fine-grained soils at distances from 2.67 m and 4.68 m, the Square Top target observed on sols 579 and 585 at distance 2.42 m and 4.47 m, and the Bonnet Plume target observed on sols 149 and 172 at distance at 3.49 m and 6.26 m. The data are normalized either to the total emission of the instrument or to the emission of each spectrometer, not withstanding, some systematic biases appear in the predictions of major elements as a function of distance. SiO_2, Al_2O_3, FeOT, NaO, K_2O, and the major-element total weight percent predictions systematically increase in value as distance increases, while the weight percent predictions of TiO_2 and CaO decrease with increasing distance. These differences are presented in Fig. 5.

The PLS model is used to predict compositions for spectra after distance correction. The spectra are considered at two distances and the observation made at the larger measurement distance is corrected to the distance of the shorter measurement distance. By correcting one observation to another observation the convergence of the two provides a metric for the success of the correction. Fig. 5 gives the predicted oxide weight percent with and without correction and the residual difference between predictions for the same target with and without correction. Percentage improvement refers to the improvement from uncorrected to corrected and is the percent that the residual difference of PLS prediction moves towards zero after correction. For the Square Top and the fine-grained soils target there is improvement for SiO_2, Al_2O_3, FeOT, CaO, Na_2O, K_2O, and total weight percent predicted. The specific improvement depends on the specific settings chosen within the model. For an optimum predetermined fixed number of components the SiO_2, Al_2O_3, FeOT, CaO, Na_2O, and K_2O improvements are 27, 16, 18, 40, 23, and 12%, respectively. The predicted improvement of the major-element total is 17%. MgO is not effectively corrected, and TiO_2 is inconsistent when

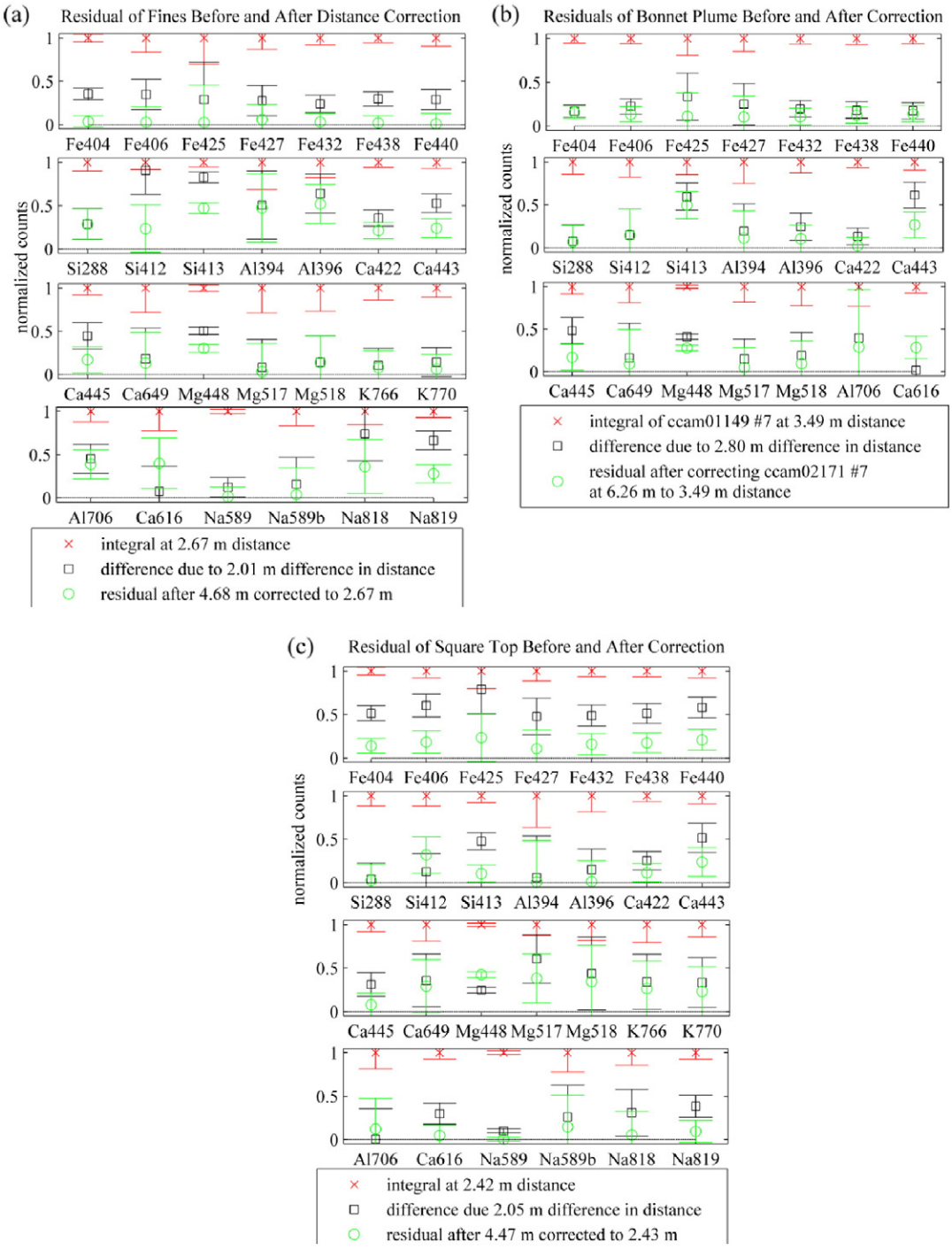

Fig. 4. Normalized peak areas of each emission line observed at the near distance. The difference plotted as a square is the original difference in emissions at the two measurement differences. The residual is the remaining difference in emissions after correction. The integral of the emission, the difference before correction and the residual are normalized by the integral value of the emission. (a) Fines at 4.68 m to 2.67 m (b) Bonnet Plume: 7th observation point at 6.26 m to the 7th observation point at 3.49 m (c) Square Top at 4.47 m to 2.43 m.

corrected, reducing differences in predictions of TiO_2 for Square Top, but not the fine-grained soils or Bonnet Plume. Although we have attempted to correct the most relevant and intense emission lines to PLS loadings, the fact that only a few of the total emission lines were corrected for distance may factor into the partial correction for these elements. In this work, we have used the ratios of elements listed in Table 2, including Fe 260 nm and Ca 397 nm, which do not show a consistent behavior with distance as indicated in Table 1. Despite this behavior, the results for FeOT and CaO are very encouraging. However, we do expect better results when we use different emission lines.

In mid-2015 the ChemCam team adopted a new calibration model that is based on weighted averages of both PLS and independent component analysis (ICA). Results presented above are sensitive to calibration model. However, there are still clear distance-related effects that should be corrected.

One drawback of the current method is that it corrects one individual emission line at a time, while the multivariate techniques of PLS and ICA investigate all channels. An alternative to that presented here is to use a set of emission lines representing high and low activation energies to estimate a simple proxy for plasma temperature and to use that to directly correct model compositions. [39].

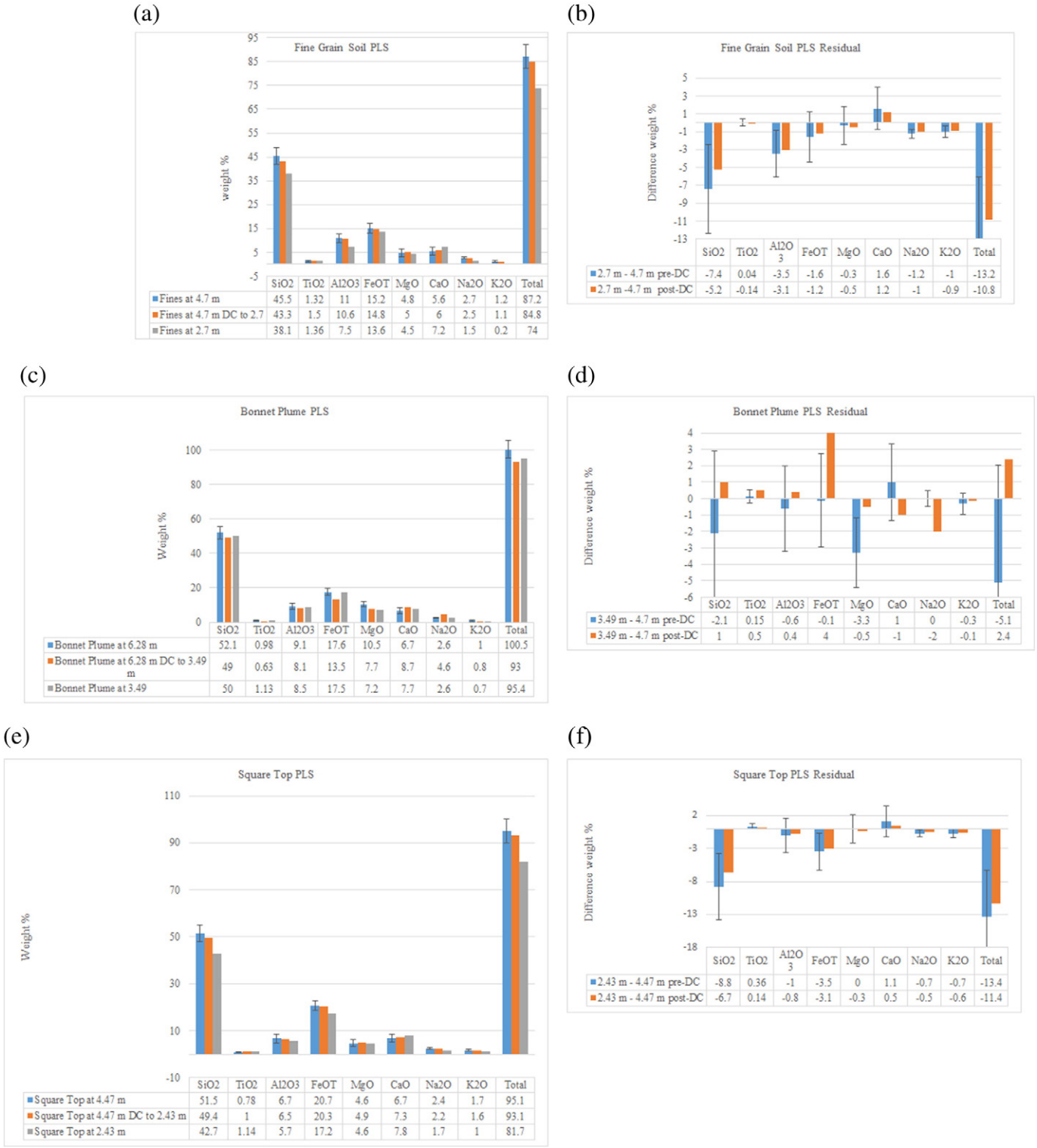

Fig. 5. PLS results with and without distance correction for fine-grain soils (a) weight percent predicted (b) residual difference between observations at different distances, Bonnet Plume (c) (d), Square Top (e) (f). Error bars represent error for each predicted oxide.

6. Conclusions

We demonstrate a combined approach using calibration curves from a proxy spectroscopic standard derived from dust measurements of many martian targets and the average behavior of the LANL Distance Calibration Suite. We have tested the use of these calibration curves to correct for distance effects on ChemCam LIBS measurements on Martian targets. These tests show that the proposed distance correction approach yields an improved agreement between ChemCam spectra of the same target obtained at different distances. In terms of quantification, the distance calibration model works to correct prediction biases at a 12% to 40% level for a number of major elements determined from martian LIBS spectra. A number of oxides can be improved but others should be excluded, namely MgO and TiO_2. The lack of correction for

MgO and TiO2 predictions is attributable to the fact that only few Mg emission lines and no Ti emission lines were distance corrected.

The distance correction presented here is still only partial. The model presented previously [27] investigated 16 emission lines. We have expanded the investigation to 27 lines, increasing the coverage from 6% to 10% of the characterized LIBS emission lines within dust spectra. With consideration of more data from Mars and from the laboratory, we see from the starting set of 75 lines (Table 1) representing 28% of total emissions in Martian dust that not all of these lines have consistent behavior across samples. This complexity limits our ability to fully correct ChemCam spectra with the method given here. These inconsistent lines will need to be addressed under a different paradigm if they are to be corrected.

This approach based on proxy spectroscopic standards further developed and tested on instrument data provides a self-contained approach for proxy standard calibration of field data for the lines described here as well behaved. This method is applicable to extraterrestrial soils and rocks as well as for Earth-based remote LIBS measurements. This technique is applicable to multivariate and univariate analyses. The method may be more effective for univariate analyses, given that a number of emission peaks covered in the multivariate analyses are not corrected, with the potential consequence that elements with a large number of emission lines (e.g., Fe, Ti, Ca, Mg) are not well corrected for distance using PLS. Distance effects will have a limited impact on much of the ChemCam LIBS data due to the fact that much of the data is taken relatively close to 3 m. About 30% of targets were shot at distances above 4 m and are candidates for distance correction. Distance correction will improve the accuracy of long-distance and short-distance targets when implemented.

Acknowledgments

This work is supported by the NASA grants (NNX09AU90A and NNX15AP84A) and the Delaware Space Grant (NNX10AN63H).

References

[1] R.E. Russo, Laser ablation, Focal Point 49 (9) (1995) 14A–28A.
[2] D.A. Cremers, L.J. Radziemski, Handbook of Laser-induced Breakdown Spectroscopy, First ed. Wiley, England, 2006.
[3] A.W. Miziolek, V. Palleschi, I. Schechter, Laser-induced Breakdown Spectroscopy (LIBS) Fundamentals and Applications, Cambridge University Press, New York, 2008.
[4] Leon Radziemski, David Cremers, A brief history of laser-induced breakdown spectroscopy: from the concept of atoms to LIBS 2012, Spectrochim. Acta B 87 (2013) 3–10.
[5] Russell S. Harmon, Richard E. Russo, Richard R. Hark, Applications of laser-induced breakdown spectroscopy for geochemical and environmental analysis: a comprehensive review, Spectrochim. Acta B (2013) (xxx, xxx–xxx).
[6] D. Cremers, The analysis of metals at a distance Using laser-induced breakdown spectroscopy, Appl. Spectrosc. 41 (1987) 572–579.
[7] Cristina Lopez-Moreno, Santiago Palanco, J. Javier Laserna, Frank DeLucia Jr., Andrzej W. Miziolek, Jeremy Rose, Roy A. Walters, Andrew I. Whitehouse, Test of a stand-off laser-induced breakdown spectroscopy sensor for the detection of explosive residues on solid surfaces, J. Anal. At. Spectrom. 21 (1) (2006) 55–60.
[8] O. Samek, D.C.S. Beddows, J. Kaiser, S.V. Kukhlevsky, M. Liska, H.H. Telle, J. Young, Application of laser-induced breakdown spectroscopy to in-situ analysis of liquid samples, Opt. Eng. 39 (2000) 2248–2262.
[9] H.L. Xu, G. Méjean, W. Liu, Y. Kamali, J.-F. Daigle, A. Azarm, P.T. Simard, P. Mathieu, G. Roy, J.-R. Simard, S.L. Chin, Remote detection of similar biological materials using femtosecond filament-induced breakdown spectroscopy, Appl. Phys. B 87 (2007) 151–156.
[10] A. Giakoumaki, K. Melessanaki, D. Anglos, Laser-induced breakdown spectroscopy (LIBS) in Archaeological Science—applications and prospects, Anal. Bioanal. Chem. 387 (2007) 749–760.
[11] J.R. Thompson, R.C. Wiens, S.M. Clegg, J.E. Barefield, D.T. Vaniman, H.E. Newsom, Remote laser induced breakdown spectroscopy (LIBS) analyses of DaG 476 and Zagami martian meteorites, Lunar Planet. Sci. XXXVII (2006) (1761.pdf).
[12] J. Lasue, R.C. Wiens, S.M. Clegg, D.T. Vaniman, K.H. Joy, S. Humphries, A. Mezzacappa, N. Melikechi, R.E. McInroy, S. Bender, Remote laser-induce breakdown spectroscopy (LIBS) for lunar exploration, J. Geophys. Res. 117 (2012) 1991–2012.
[13] A.I. Whitehouse, Laser-induced breakdown spectroscopy and its application to the remote characterization of hazardous materials, Spectrosc. Eur. 18 (2006) 14–21.
[14] V. Sautter, et al., Igneous mineralogy at Bradbury Rise: the first ChemCam campaign at Gale crater, J. Geophys. Res. Planets 119 (1) (2014) 30–46.
[15] S.M. McLennan, et al., Elemental geochemistry of sedimentary rocks at Yellowknife Bay, Gale crater, Mars, Science 343 (6169) (2014) 1244734.
[16] R.B. Anderson, J.C. Bridges, A. Williams, L. Edgar, A. Ollila, J. Williams, M. Nachon, N. Mangold, J. Schieber, S. Gupta, G. Dromart, R.C. Wiens, S. Le Mouelic, O. Forni, N. Lanza, A. Mezzacappa, V. Sautter, M. Fisk, D. Blaney, B. Clark, S. Clegg, O. Gasnault, J. Lasue, R. Leveillé, E. Lewin, K.W. Lewis, S. Maurice, S.P. Schwenzer, D. Vaniman, ChemCam results from the Shaler outcrop in Gale crater, Mars, Icarus 249 (2015) 2–21, http://dx.doi.org/10.1016/j.icarus.2014.07.025.
[17] P.-Y. Meslin, O. Gasnault, O. Forni, S. Schröder, G. Berger, A. Cousin, S. Clegg, J. Lasue, V. Sautter, S. Maurice, S. Le Mouélic, R. Wiens, C. Fabre, W. Goetz, N. Mangold, B. Ehlmann, N. Lanza, D. Bish, A.-M. Harri, R. Anderson, E. Rampe, T.H. McConnochie, P. Pinet, R. Léveillé, D. Archer, B. Barraclough, S. Bender, D. Blake, D. Blaney, J. Blank, N. Bridges, B. Clark, D. Delapp, G. Dromart, M.D. Dyar, M. Fisk, B. Gondet, J. Grotzinger, K. Herkenhoff, J. Johnson, J.-L. Lacour, Y. Langevin, L. Leshin, E. Lewin, M.B. Madsen, N. Melikechi, A. Mezzacappa, J.E. Moores, H. Newsom, A. Ollila, R. Perez, N. Renno, J.-B. Sirven, R. Tokar, M. de la Torre, L. d'Uston, D. Vaniman, A. Yingst, the MSL Science Team, Soil diversity and hydration as observed by ChemCam at Gale Crater, Mars, Science 341 (6153) (2013) 1238670.
[18] A. Cousin, P.Y. Meslin, R.C. Wiens, W. Rapin, N. Mangold, C. Fabre, O. Gasnault, O. Forni, R. Tokar, A. Ollila, S. Schröder, J. Lasue, S. Maurice, V. Sautter, H. Newsom, D. Vaniman, S. Le Mouélic, D. Dyar, G. Berger, D. Blaney, M. Nachon, G. Dromart, N. Lanza, B. Clark, S. Clegg, W. Goetz, J. Berger, B. Barraclough, D. Delapp, MSL Science Team, Compositions of coarse and fine particles in martian soils at gale: A window into the production of soils, Icarus 249 (2015) 22–42.
[19] B. Sallé, P. Mauchien, S. Maurice, Laser-induced breakdown spectroscopy in open-path configuration for the analysis of distant objects, Spectrochim. Acta B 62 (2007) 739–768.
[20] I. Gaona, J. Moros, J.J. Laserna, New insights into the potential factors affecting the emission spectra variability in standoff LIBS, J. Anal. At. Spectrom. 28 (2013) 1750–1759.
[21] José M. Vadillo, Pedro L. García, Santiago Palanco, D. Romero, José Ma Baena, J. Javier Laserna, Remote, real-time, on-line monitoring of high-temperature samples by noninvasive open-path laser plasma spectrometry, Anal. Bioanal. Chem. 375 (2003) 1144–1147.
[22] Santiago Palanco, Cristina Lo'pez-Moreno, J. Javier Laserna, Design, construction and assessment of a field-deployable laser-induced breakdown spectrometer for remote elemental sensing, Spectrochim. Acta B 61 (2006) 88–95.
[23] J.A. Aguilera, C. Aragón, Characterization of laser-induced plasmas by emission spectroscopy with curve-of-growth measurements. Part II: effect of the focusing distance and the pulse energy, Spectrochim. Acta B 63 (2008) 793–799.
[24] R.A. Multari, L.E. Foster, D.A. Cremers, M.J. Ferris, Effect of sampling geometry on elemental emissions in laser-induced breakdown spectroscopy, Appl. Spectrosc. 50 (1996) 1483–1499.
[25] J.A. Aguilera, C. Aragon, Characterization of laser-induced plasma by spatially resolved spectroscopy of neutral atom and ion emissions. Comparison of local and spatially integrated measurements, Spectrochim. Acta B 59 (2004) 1861–1876.
[26] G.G.A. de Carvalho, D.S. Junior, L.C. Nunes, M.D. Gomes, F.D. Leme, F.J. Krug, Effects of laser focusing and fluence on the analysis of pellets of plant materials by laser-induced breakdown spectroscopy, Spectrochim. Acta B 74–75 (2012) 162–168.
[27] N. Melikechi, A. Mezzacappa, A. Cousin, N.L. Lanza, J. Lasue, S.M. Clegg, G. Berger, R.C. Wiens, S. Maurice, R.L. Tokar, S. Bender, O. Forni, E.A. Breves, M.D. Dyar, J. Frydenvang, D. Delapp, O. Gasnault, H. Newsom, A.M. Ollila, E. Lewin, B.C. Clark, B.L. Ehlmann, D. Blaney, C. Fabre, Correcting for variable laser-target distances of LIBS measurements with ChemCam using emission lines of Martian dust spectra, Spectrochim. Acta B 96 (2014) 51–60.
[28] N. Mangold, O. Forni, A. Ollila, R. Anderson, G. Berger, J. Bridges, S. Clegg, A. Cousin, W. Dietrich, G. Dormart, S. Gupta, E. Lewin, C. Fabre, O. Gasnault, S. Le Mouelic, S. Maurice, P.-Y. Meslin, V. Sautter, R. Wiens, The MSL Science Team, ChemCam analysis of conglomerates at Bradbury site, Mars, EGU General Assembly Conference Abstracts, 15 Apr. 2013, p. 2214.
[29] P.-Y. Meslin, O. Gasnault, O. Forni, S. Schröder, A. Cousin, G. Berger, S. Clegg, J. Lasue, S. Maurice, V. Sautter, S. Le Mouélic, R. Wiens, C. Fabré, W. Goetz, D. Bish, N. Mangold, B. Ehlmann, N. Lanza, A.-M. Harri, R. Anderson, E. Rampe, T.H. McConnochie, P. Pinet, D. Blaney, R. Léveillé, D. Archer, B. Barraclough, S. Bender, D. Blake, J.G. Blank, N. Bridges, B.C. Clark, L. DeFlores, D. Delapp, G. Dromart, M.D. Dyar, M. Fisk, B. Gondet, J. Grotzinger, K. Herkenhoff, J. Johnson, J.-L. Lacour, Y. Langevin, L. Leshin, E. Lewin, M.B. Madsen, N. Melikechi, A. Mezzacappa, M.A. Mischna, J.E. Moores, H. Newsom, A. Ollila, R. Perez, N. Renno, J.-B. Sirven, R. Tokar, M. de la Torre, L. d'Uston, D. Vaniman, A. Yingst, the MSL Science Team, Soil diversity and hydration as observed by ChemCam at Gale crater, Mars, Science 341 (2013) 1476, http://dx.doi.org/10.1126/science.1238670 (full text online).
[30] S. Maurice, R.C. Wiens, M. Saccoccio, B. Barraclough, O. Gasnault, O. Forni, N. Mangold, D. Baratoux, S. Bender, G. Berger, J. Bernardin, M. Berthé, N. Bridges, D. Blaney, M. Bouyé, P. Caïs, B. Clark, S. Clegg, A. Cousin, D. Cremers, A. Cros, L. DeFlores, C. Derycke, B. Dingler, G. Dromart, B. Dubois, M. Dupieux, E. Durand, L. d'Uston, C. Fabre, B. Faure, A. Gaboriaud, T. Gharsa, K. Herkenhoff, E. Kan, L. Kirkland, D. Kouach, J.-L. Lacour, Y. Langevin, J. Lasue, S. Le Mouélic, M. Lescure, E. Lewin, D. Limonadi, G. Manhès, P. Mauchien, C. McKay, P.-Y. Meslin, Y. Michel, E. Miller, H.E. Newsom, G. Orttner, A. Paillet, L. Parès, Y. Parot, R. Pérez, P. Pinet, F. Poitrasson, B. Quertier, B. Sallé, C. Sotin, V. Sautter, H. Séran, J.J. Simmonds, J.-B. Sirven, R. Stiglich, N. Striebig, J.-J. Thocaven, M.J. Toplis, D. Vaniman, The ChemCam instrument suite on the Mars Science Laboratory (MSL) Rover: science objectives and mast unit description, Space Sci. Rev. 170 (2012) 95–166.

[31] R.C. Wiens, S. Maurice, B. Barraclough, M. Saccoccio, W.C. Barkley, J.F. Bell III, S. Bender, J. Bernardin, D. Blaney, J. Blank, M. Bouye, N. Bridges, N. Bultman, P. Cais, R.C. Clanton, B. Clark, S.M. Clegg, A. Cousin, D.A. Cremers, A. Cros, L. DeFlores, D. Delapp, R. Dingler, C. D'Uston, M.D. Dyar, T. Elliott, D. Enemark, C. Fabre, M. Flores, O. Forni, O. Gasnault, T. Hale, C. Hays, K. Herkenhoff, E. Kan, L. Kirkland, D. Kouach, D. Landis, Y. Langevin, N. Lanza, F. LaRocca, J. Lasue, J. Latino, D. Limonadi, C. Lindensmith, C. Little, N. Mangold, G. Manhes, P. Mauchien, C. McKay, E. Miller, J. Mooney, R.V. Morris, L. Morrison, T. Nelson, H. Newsom, A. Ollila, M. Ott, L. Pares, R. Perez, F. Poitrasson, C. Provost, J.W. Reiter, T. Roberts, F. Romero, V. Sautter, S. Salazar, J.J. Simmonds, R. Stiglich, S. Storms, N. Striebig, J.-J. Thocaven, T. Trujillo, M. Ulibarri, D. Vaniman, N. Warner, R. Waterbury, R. Whitaker, J. Witt, B. Wong-Swanson, The ChemCam instrument suite on the Mars Science Laboratory (MSL) Rover: body unit and combined system tests, Space Sci. Rev. 170 (2012) 167–227.
[32] V.E. Hamilton, H.Y. McSween Jr., B. Hapke, Mineralogy of Martian atmospheric dust inferred from thermal infrared spectra of aerosols, J. Geophys. Res. 110 (2005) 2156–2202.
[33] M.W. Liemohn, A. Dupre, S.W. Bougher, M. Trantham, D.L. Mitchell, M.D. Smith, Time-history influence of global dust storms on the upper atmosphere on Mars, Geophys. Res. Lett. 39 (2012) 1944–8007.
[34] C. Aragon, J.A. Aguilera, F. Penalba, Improvements in quantitative analysis of steel composition by laser-induced breakdown spectroscopy at atmospheric pressure using an infrared Nd:YAG laser, Appl. Spectrosc. 53 (1999) 1259–1267.
[35] R.C. Wiens, S. Maurice, J. Lasue, O. Forni, R.B. Anderson, S. Clegg, S. Bender, D. Blaney, B.L. Barraclough, A. Cousin, L. Deflores, D. Delapp, M.D. Dyar, C. Fabre, O. Gasnault, N. Lanza, J. Mazoyer, N. Melikechi, P.-Y. Meslin, H. Newsom, A. Ollila, R. Perez, R.L. Tokar, D. Vaniman, Pre-flight calibration and initial data processing for the ChemCam laser-induced breakdown spectroscopy instrument on the Mars Science Laboratory rover, Spectrochim. Acta B 82 (2013) 1–27.
[36] P. Gill, W. Murray, M. Wright, Practical Optimization, 6th ed. Academic Press, London, 1981.
[37] B.L. Ehlmann, D.L. Bish, S.W. Ruff, J.F. Mustard, Mineralogy and chemistry of altered Icelandic basalts: application to clay mineral detection and understanding aqueous environments on Mars, J. Geophys. Res. E Planets 117 (2012) 1–27.
[38] S.M. Clegg, E. Sklute, M.D. Dyar, J.E. Barefield, R.C. Wiens, Multivariate analysis of remote laser-induced breakdown spectroscopy spectra using partial least squares, principle component analysis, and related techniques, Spectrochim. Acta B 64 (2009) 79–88.
[39] R.L. Tokar, R.C. Wiens, S. Maurice, A. Pilleri, R. Gellert, R.B. Anderson, S.C. Bender, S.M. Clegg, M.D. Dyar, C. Fabre, O. Forni, O. Gasnault, J. Lasue, N. Melikechi, Relationship between MSL/ChemCam laser focus, plasma temperature, and compositional calibrations, Lunar Planet. Sci. XLVI (2015) 1369 (The Lunar and Planetary Institute, Houston, TX).